



**HAL**  
open science

# Reconstructing lake bottom water temperatures and their seasonal variability in the Dead Sea Basin during MIS5e

Niels Brall, Véronique Gardien, Daniel Ariztegui, Philippe Sorrel, Emmanuel Guillerm, Frédéric Caupin

► **To cite this version:**

Niels Brall, Véronique Gardien, Daniel Ariztegui, Philippe Sorrel, Emmanuel Guillerm, et al.. Reconstructing lake bottom water temperatures and their seasonal variability in the Dead Sea Basin during MIS5e. *Depositional Record*, 2022, 10.1002/dep2.185 . hal-03602331

**HAL Id: hal-03602331**

**<https://hal.science/hal-03602331v1>**

Submitted on 9 Mar 2022

**HAL** is a multi-disciplinary open access archive for the deposit and dissemination of scientific research documents, whether they are published or not. The documents may come from teaching and research institutions in France or abroad, or from public or private research centers.

L'archive ouverte pluridisciplinaire **HAL**, est destinée au dépôt et à la diffusion de documents scientifiques de niveau recherche, publiés ou non, émanant des établissements d'enseignement et de recherche français ou étrangers, des laboratoires publics ou privés.



Distributed under a Creative Commons Attribution 4.0 International License

## ORIGINAL ARTICLE

# Reconstructing lake bottom water temperatures and their seasonal variability in the Dead Sea Basin during MIS5e

Niels S. Brall<sup>1,2</sup>  | Véronique Gardien<sup>1</sup>  | Daniel Ariztegui<sup>3</sup>  | Philippe Sorrel<sup>1</sup>  | Emmanuel Guillerm<sup>1,2</sup>  | Frédéric Caupin<sup>2</sup> 

<sup>1</sup>Laboratoire de Géologie de Lyon: Terre, Planètes et Environnement, Université Claude Bernard Lyon 1, CNRS, Université de Lyon, Villeurbanne, France

<sup>2</sup>Institut Lumière Matière, Université Claude Bernard Lyon 1, CNRS, Université de Lyon, Lyon, France

<sup>3</sup>Department of Earth Sciences, University of Geneva, Geneva, Switzerland

## Correspondence

Niels S. Brall, Laboratoire de Géologie de Lyon: Terre, Planètes et Environnement, Université Claude Bernard Lyon 1, CNRS, Université de Lyon, 2 rue Raphaël Dubois, Villeurbanne, France.  
 Email: brallniels@gmail.com

## Present address

Emmanuel Guillerm, The Dr. Moses Strauss Department of Marine Geosciences, Charney School of Marine Sciences, University of Haifa, Haifa, Israel

## Funding information

Campus France, Grant/Award Number: mopga-phd-0000000160

## Abstract

Interglacial periods are characterised by thick accumulations of halite units in the Dead Sea Basin. During these intervals, small water droplets (fluid inclusions, FIs) were entrapped in the halite crystals which serve as windows to estimate the chemistry and physical properties of the primary lake water conditions. Brillouin spectroscopy is used here to reconstruct annual resolution temperatures from a halite core section in the Dead Sea Basin during the onset of Marine Isotope Stage 5e (*ca* 130 ka) of the Last Interglacial. Lake bottom temperatures can be inferred based on the occurrence of coarse/fine halite facies, as observed today with the formation of equivalent halite facies during winter/summer seasons in the Dead Sea. A recurring increase in lake bottom temperatures is found along the direction of coarse halite layers in three successive years. Moreover, low FI entrapment temperatures were detected in layers of fine (cumulate) halite facies. These results imply a twofold stronger seasonality in the Dead Sea Basin compared to today, with colder winters at the onset of Marine Isotope Stage 5e. The results therefore highlight the potential of using cyclic salt deposits to reconstruct seasonal temperature variability for numerous evaporitic environments in the geological record.

## KEYWORDS

Brillouin spectroscopy, Dead Sea Basin, fluid inclusions, marine isotope stage (MIS) 5e, palaeotemperature, seasonal halite facies

## 1 | INTRODUCTION

Palaeoclimatic reconstructions often show that long-term global climate changes are largely induced through processes and feedbacks on seasonal timescales (Denton et al., 2005; Werner et al., 2000). A substantial impact of

seasonality on various proxies has been proposed (Clemens & Prell, 2003; Huguet et al., 2006) at annual (Brocas et al., 2018; Felis et al., 2004), centennial (Bar-Matthews et al., 2003; Brauer et al., 2009) or millennial-scale resolutions (Milner et al., 2012). Continental archives such as tree rings, laminated speleothems and varved lake sediments

This is an open access article under the terms of the Creative Commons Attribution License, which permits use, distribution and reproduction in any medium, provided the original work is properly cited.

© 2022 The Authors. *The Depositional Record* published by John Wiley & Sons Ltd on behalf of International Association of Sedimentologists

can provide seasonal records of different climate variables (Baldini et al., 2021; Ben Dor et al., 2019; Shi et al., 2010). For example, laminations in speleothems commonly accumulate more calcite in the cool season and less or none during the warm season (Riechelmann et al., 2020). Analogously, varved sediments have been extensively used for the last few decades, to reconstruct, for example, seasonal rainfall intensity in temperate/periglacial lakes (Ariztegui et al., 2010), the long-term progressive lake-level decline in a hyper-arid region in northern Chad (Francus et al., 2013), both winter precipitation and temperatures in southern Finland (Ojala et al., 2013), flooding events in the Southern Alps (Wirth et al., 2013) as well as Holocene temperatures in China and Switzerland (Chu et al., 2005; Trachsel et al., 2012).

Calibration studies using the  $\delta^{18}\text{O}$  composition of modern ostracods in turn provide temperature reconstructions that are in good agreement with the observed range of seasonal changes in lake water temperature (Labuhn et al., 2021), based on ‘palaeotemperature’ equations for equilibrium carbonate precipitation and the estimated mean  $\delta^{18}\text{O}$  of lake water. However, the high intra-species carbonate  $\delta^{18}\text{O}$  variability of samples leads to a large scatter in the reconstructed temperatures often compromising palaeotemperature reconstructions. Recent progress in reconstructing palaeotemperatures has been made by using biomarkers (i.e. leaf wax *n*-alkanes, bacterial branched glycerol dialkyl glycerol tetraethers [brGDGTs]), however, these geochemical proxies include certain limitations as well (Liu & An, 2020; Wang et al., 2018). Thus, most palaeoclimate proxies provide relative changes in climate variables while a direct and precise reconstruction of such variables is still lacking. Therefore, there is a crucial need for resolving seasonal temperature variations using continental archives to improve long-term palaeoclimate reconstructions.

In this study, halite (NaCl) samples from the Dead Sea Basin (DSB) are used to reconstruct seasonal temperature variability during Marine Isotope Stage 5e (MIS5e). Today, halite precipitates on the deep hypolimnion lake floor of the DSB as alternating layers responding to a seasonal frequency (Kiro et al., 2016; Sirota et al., 2021). During their formation, NaCl crystals may trap droplets of the surrounding lake water from which they precipitate, called fluid inclusions (FIs). Recently, a new palaeothermometer based on Brillouin spectroscopy (BS) was elaborated on FIs in natural quartz (El Mekki-Azouzi et al., 2015) and laboratory-grown NaCl crystals (Guillerm et al., 2020), and used on a sedimentary core from the DSB to reconstruct temperature and lake-level changes of the Dead Sea over the Last Interglacial (LIG, 130–115 ka; Guillerm, 2019). In the present contribution, the focus is on a shorter time interval encompassing three closely spaced samples,

to reconstruct palaeotemperature variability of the lake waters at an unprecedented (i.e. seasonal) resolution.

## 2 | GEOLOGICAL SETTING AND MATERIAL

The modern Dead Sea is a hypersaline terminal lake occupying a pull-apart basin along the DSB (Smit et al., 2008) (Figure 1A). With a current water surface at 434 m below mean sea level (m bsl) receding at a rate of 1 m/year, it is nowadays the lowest exposed continental point on Earth. Located at the Levantine land bridge connecting Africa with Asia, the region is influenced by both Mediterranean climate and tropical storms surging from the Saharo-Arabian desert belt (Neugebauer et al., 2014 and references therein).

The hydrographic lake regime has been switching between meromictic (stable stratification without mixing during a year) and holomictic (lake mixing once a year) periods since 1978 (Anati et al., 1987; Gertman & Hecht, 2002). The long-term meromictic regime of the modern Dead Sea was interrupted for just 2 months with an overturn of the water body in winter 1978–1979 (Steinhorn, 1985), associated with the onset of halite precipitation on the surface in February 1979 (Steinhorn, 1983). After several switches between both regimes (meromictic phases from 1979–1982 and 1991–1995; holomictic phase from 1983–1991), perpetual holomictic conditions have prevailed since 1996 coevally with the precipitation of halite (Anati & Stiller, 1991; Anati et al., 1987; Gertman & Hecht, 2002). Moreover, seasonal-driven variations in solar radiation, temperature, quasi-salinity and the degree of halite supersaturation have been both observed and extensively studied (Arnon et al., 2016; Gertman & Hecht, 2002; Sirota et al., 2017). The main seasonal feature is a well-mixed water body from surface to bottom during the winter season between late November and early March (Gertman & Hecht, 2002), and a thermal stratification from early spring to late fall (Gertman & Hecht, 2002). Modern halite precipitation is characterised by (1) bottom-grown coarse halite (mainly spring–late summer) and (2) floating fine cumulate halite that nucleates in the whole water column excessively during winter due to a high supersaturation of halite, and to a minor extent during summer below the thermocline (Sirota et al., 2017).

The DSB has been successively occupied by several lakes and water bodies since the first marine incursion from the Mediterranean Sea during the Miocene (Neev & Emery, 1967; Stein, 2001). The current study focusses on the sediments from Lake Samra, which was the last interglacial (*ca* 129–116 ka) precursor of the Dead Sea (Waldmann et al., 2009). The first long sedimentary core covering

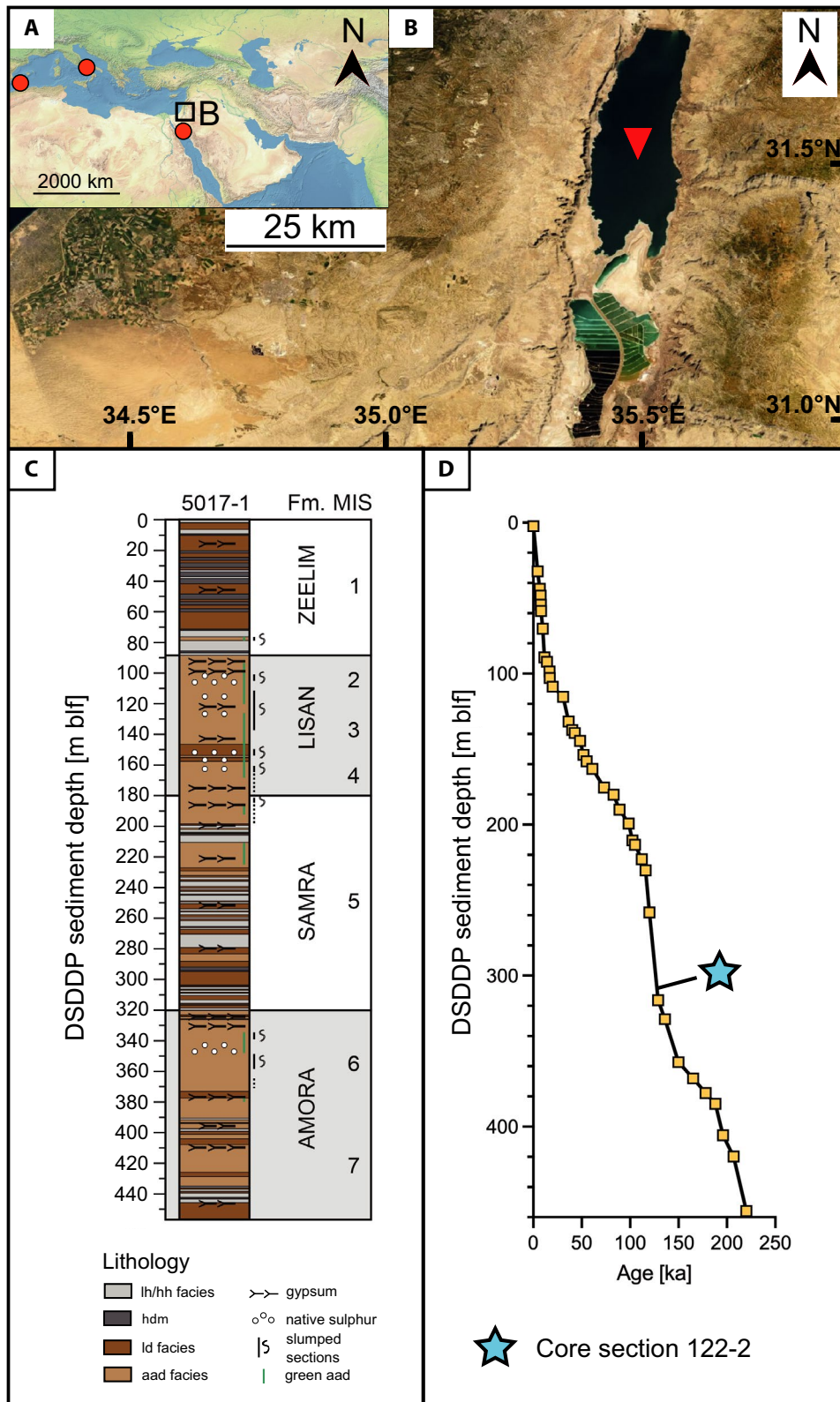


**FIGURE 1** (A and B) Location of Dead Sea, middle East, with DSDDP site (red triangle) and study sites referred to in the discussion (red circles). (C) Lithological profile of DSDDP core 5017-1-A with related formations (Fm.) and Marine Isotope Stages (MIS) (from Ben Dor et al., 2019; modified after Neugebauer et al., 2014). (D) Revised age model for DSDDP core 5017-1-A after Goldstein et al. (2020), sampled core section indicated by blue star



this time interval was retrieved within the framework of an International Continental Drilling Program (ICDP)-sponsored initiative (5017-1-A) (Neugebauer et al., 2014; Stein et al., 2011) (Figure 1C). In this core, a layered halite facies ('lh') accounts for around 20% of the sedimentary sequence and is composed of alternating grey marl laminae (<1 mm), fine cumulate halite (0.2–4 cm; termed 'CU') and coarse halite (1–10 mm; termed 'CO') (Neugebauer et al., 2014). Core section interval 5017-1-A-122-A-2 (315.17–315.03 m below lake floor, m blf) yields four continuous segments of such cumulate-coarse halite alternations, enclosed by *ca* 4–10 cm thick mud intervals (Figure 2A). Three of these halite alternations were investigated in the present study (Figure 2A). Furthermore, the whitish cumulate halite layers are characterised by assemblages of single NaCl grains *ca* 150–400  $\mu$ m in size containing dense fluid inclusions bands (FIBs) around a central FI-free zone (Figure 2D). Conversely, dark-grey coarse layers encompass cubic single NaCl crystals with grain sizes of *ca* 5 mm (Figure 2B). Milky/cloudy FIB in coarse samples represent primary FIs that have been entrapped during crystal growth (Figure 2B) with sizes varying from 1 to 40  $\mu$ m (Figure 2C).

A recently improved age model for core 5017-1-A (Figure 1D) includes a new tie point at 129 ka  $\pm$  1 ka at 316.24 m blf (i.e. close to the bottom core section at

315.17 m blf), which therefore corresponds to the onset of MIS5e during the last interglacial period (Goldstein et al., 2020).

### 3 | METHODS

Sampling of core section 5017-1-A-122-A-2 was carried out at GFZ Potsdam (Germany). Selected pieces of halite crystals were placed on their flat side on a microscope cover slip in a temperature-controlled stage (Linkam THMS 600) with 0.1°C resolution. Samples were studied with an upright optical microscope (Zeiss Axio Imager. Z2 Vario), equipped with a long-working distance  $\times$ 100 objective (Mitutoyo Plan-Apo, N.A. 0.7). To select suitable FIs for analysis, published criteria for accurate Brillouin analysis on halite crystals (Guillerm et al., 2020) was followed. For palaeothermometry, the previously described full set-up and detailed physical principles of BS were used (El Mekki-Azouzi et al., 2015).

The method is based on the measurement of sound velocity ( $w$ ) in a liquid which depends on the composition, temperature ( $T$ ) and pressure of the liquid. When heated or cooled, a monophasic FI (only liquid) follows an isochore at constant volume, along which  $w$  varies with  $T$ . In a biphasic FI (liquid + vapour),  $w$  of the liquid is

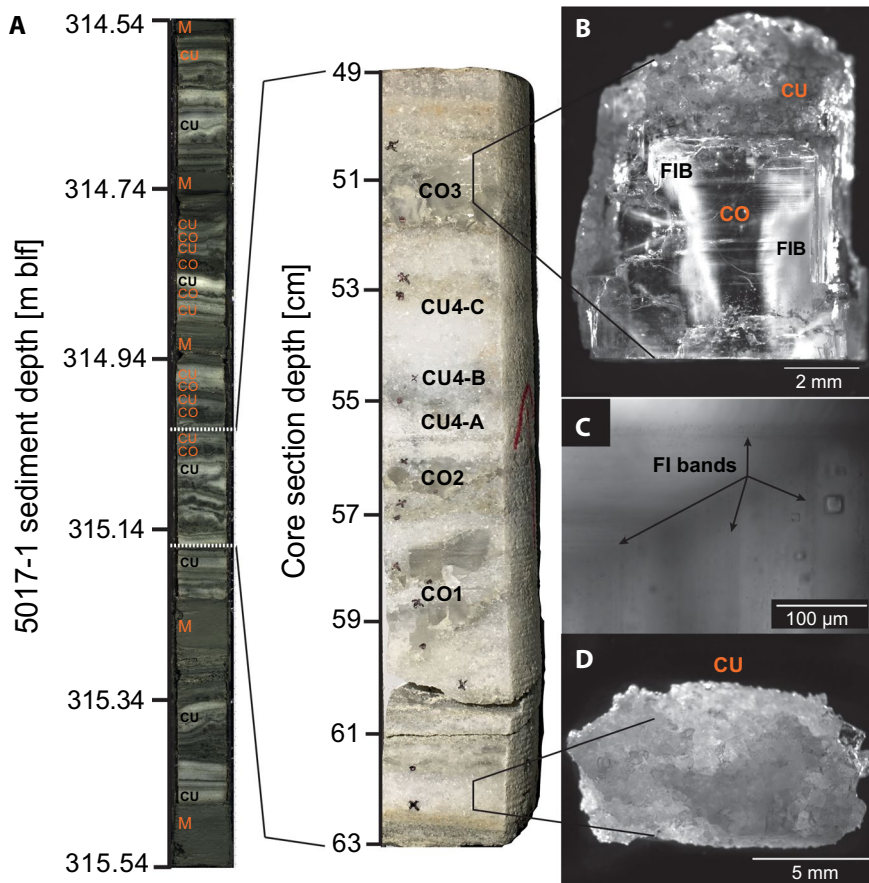


**FIGURE 2** (A) Left, image of core section 122-2 with alternations of mud (M), cumulate (CU) and coarse (CO) facies. Right, image of coarse-cumulate depositional cycles. (B) CO and CU crystals, separated by a sharp transition that indicates a change in hydrological lake conditions. Peculiar cloudy fluid inclusion bands (FIB) in CO. (C) Common primary FIB from sample CO2-BOT. (D) CU assemblages bounded by countless single CU crystals

measured as a function of  $T$  at the solid–liquid–vapour equilibrium (SLVE). Hence, a transformation (cavitation) from a monophasic phase into a biphasic phase is required for each FI and achieved by a short-term thermal cycle (Figure S1). By definition, for a FI trapped near ambient pressure (0.1 MPa), the crossing temperature  $T_x$  equals the entrapment temperature  $T_f$  at which both  $w$  curves intersect (along both the isochore and SLVE; Figures S1 and S2).

A value for one fluid inclusion (FI) consists of eight single measurements conducted at different temperatures to establish both an isochore (monophasic FI) and a solid–liquid–vapour equilibrium (SLVE; biphasic FI) curve (Figure S1). The intersection of both curves is defined as  $T_x$  (Figure S2). To obtain biphasic FIs, large temperature excursions are necessary by means of an increase from room temperature to +130°C, then back to room temperature. This causes plastic deformation of the salt host crystal with an increase in volume, forcing cavitation of a vapour bubble in the FIs. At this point, the FIs enters the stability field and represents ambient pressure conditions (Figure S1). During the cavitation process, the chemical composition of an individual fluid inclusion does not change.

Data are presented here as mean  $T_x$  values for each sub-section (i.e. uppermost samples in coarse layers, labelled ‘CO-TOP’ and lowermost samples in coarse layers labelled ‘CO-BOT’).

Each mean  $T_x$  value is calculated by the mean of all measured FIs:

$$\text{Mean } T_x = \frac{\sum x_i}{N} \quad (1)$$

with  $x_i$  the  $T_x$  value for  $FI_i$  and  $N$  the number of all FIs. Mean  $T_x$  values are analysed statistically by means of their standard deviation (SD), derived from Equation 2:

$$SD = \sqrt{\frac{\sum (x_i - \text{Mean } T_x)^2}{N - 1}} \quad (2)$$

The standard error of the mean (SE), used as error bars in each figure, is calculated by Equation 3:

$$SE = \frac{SD}{\sqrt{N}} \quad (3)$$

To rule out post-entrapment processes in the samples, histograms were used to check for statistical distributions that are close to Gaussian distributions (Figure S3).

A correction term was applied on measured  $T_x$  data according to the pressure of the water column above where crystals form ( $T_f = T_x + \Delta T_p$ , with  $\Delta T_p = 4.8^\circ\text{C}$  for crystals

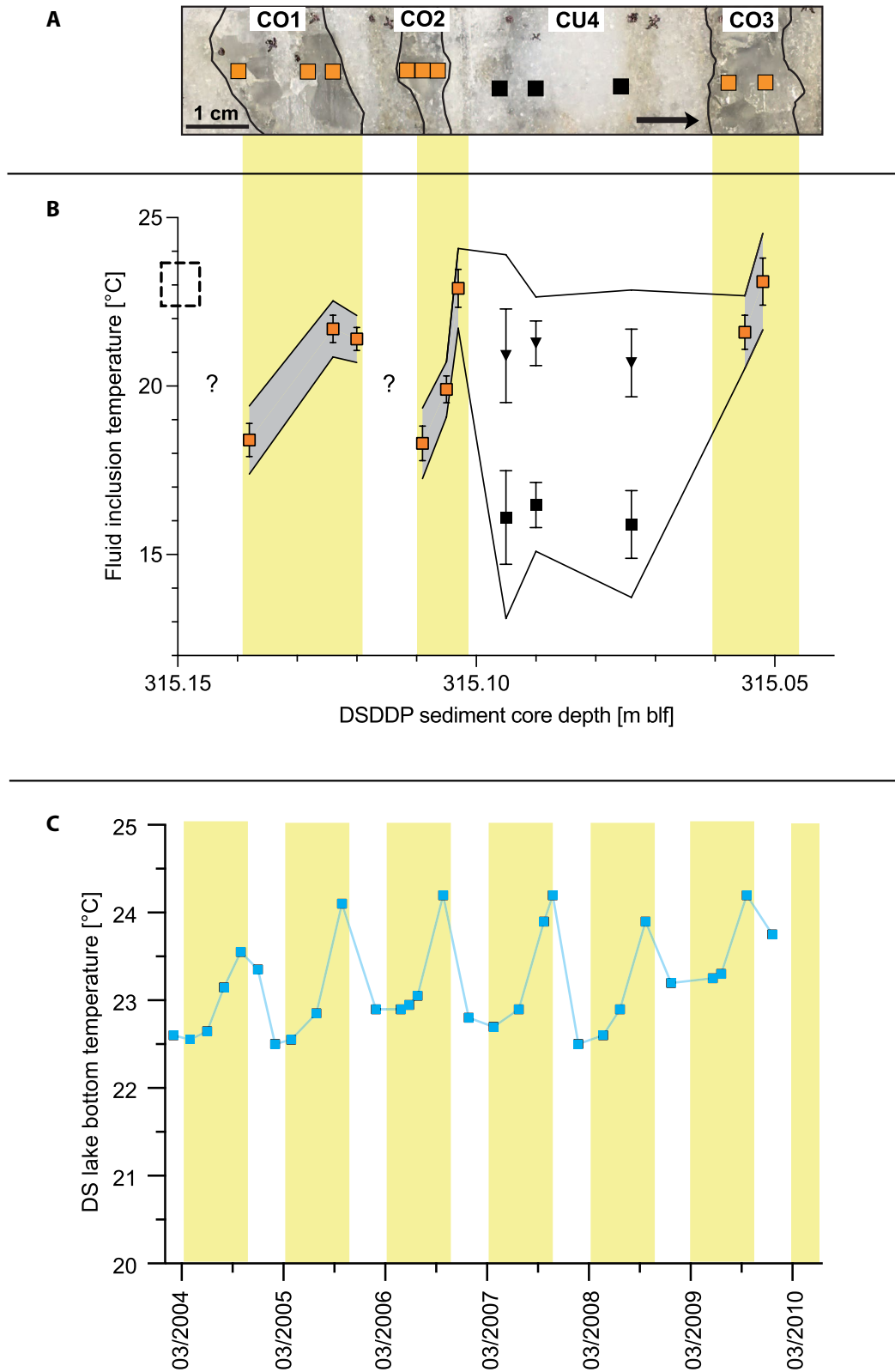
precipitated at lake bottom). Here, a water column height of 539 m was calculated based on a pressure of 6.45 MPa and a lake level of –250 m above sea level (Guillerm, 2019). Such a reconstructed lake-level value, based on speed of sound measurements in biphasic FIs (Guillerm, 2019), is similar to that of a recently published synthetic lake level for the beginning of the Last Interglacial (Torfstein et al., 2013). It is noteworthy to mention that, as the coarse halite layers studied here were deposited during a short time interval, the pressure correction is virtually equal for all of them. Therefore, any difference between uncorrected  $T_x$  can be directly converted into a difference between  $T_f$  values. Conversely, as cumulate halite crystals form in the water column between the surface and the bottom of the lake the unknown  $T$  correction for formation depth is less or equal to the  $T$  correction for coarse halite crystals. Therefore, in view of the  $T_x$  values, the  $T_f$  of cumulate halite layers must be less than the  $T_f$  for the surrounding coarse halite layers.

## 4 | RESULTS

Individual  $T_x$  of FIs were measured in three successive CO halite layers (CO1, CO2, CO3) (Figure 3A) with increasing core depths (from 315.138 to 315.052 m blf, Table 1). Additionally, the  $T_x$  of FIs were measured in one fine CU layer (CU4) that deposited prior to the youngest CO3 halite layer (CO3-BOT) (Figure 3A). Here the pressure-corrected temperature ( $T_f$ ), with reported uncertainties as standard error of the mean (SE), is reported for each interval. The deepest and oldest layer CO1 has been divided into three sub-sections (total number of measured FIs  $n = 103$ ) with  $T_f$  values of  $18.4 \pm 0.5^\circ\text{C}$ ,  $21.7 \pm 0.4^\circ\text{C}$  and  $21.4 \pm 0.4^\circ\text{C}$  for CO1-BOT, CO1-MID and CO1-TOP, respectively. The second CO layer CO2 is divided into three sub-sections ( $n = 90$ ).  $T_f$  values vary from  $18.3 \pm 0.5^\circ\text{C}$ ,  $19.9 \pm 0.4^\circ\text{C}$  and  $22.9 \pm 0.6^\circ\text{C}$  for CO2-BOT, CO2-MID and CO2-TOP respectively (Figure 3B).

The uppermost and relatively youngest CO layer CO3, divided into two sub-sections, base and top ( $n = 48$ ), provides  $T_f$  values of  $21.6 \pm 0.5^\circ\text{C}$  and  $23.1 \pm 0.7^\circ\text{C}$  for CO3-BOT and CO3-TOP respectively (Table 1, Figure 3B). This dataset shows that mean  $T_f$  values in each CO layer increase with increasing layer thickness from base to top. A clear difference in  $T_f$  values is therefore observed by separating the dataset into groups of only coarse-bottom and coarse-top values, which reveals that lowest temperatures correspond to samples from the coarse-bottom layers, while highest temperatures are found only in coarse-top layers (Figure 4).

Three CU sub-samples provide uncorrected  $T_x$  values of  $16.1 \pm 1.4^\circ\text{C}$  ( $n = 14$ ),  $16.5 \pm 0.7^\circ\text{C}$  ( $n = 26$ ) and



$15.9 \pm 1.0^{\circ}\text{C}$  ( $n = 15$ ) for CU4-A, CU4-B and CU4-C respectively (Table 1, Figure 3B). Hence, those temperatures are lower than both surrounding uncorrected  $T_x$  values of CO layers with  $16.8$  and  $18.1^{\circ}\text{C}$  for CO3-BOT and CO2-TOP respectively (Figure S4). As cumulate crystals form

in the water column between the surface and the bottom of the lake, the unknown temperature correction is less or equal to the temperature correction for coarse crystals. Therefore, the  $T_f$  of these cumulate crystals must be less than the  $T_f$  for the surrounding coarse halite layers.

**FIGURE 3** (A) Annually deposited halite layers in core section 5017-1-A-122-2. Black lines mark facies boundaries between layers of coarse halite (CO) and cumulate halite (CU). Sampling locations of CO (orange squares) and CU (black squares) indicated. Growth direction indicated by black arrow. (B) Reconstructed entrapment temperatures of halite layers: corrected coarse  $T_f$  data (orange squares), uncorrected cumulate  $T_x$  data (black squares), and corrected cumulate  $T_f$  data (triangles) to show the large uncertainty of Brillouin spectroscopy for cumulate halite samples. Thus, all cumulate data should be considered with caution when interpreting their palaeoseasonal implications. Dashed black box at y-axis exhibits monitored deep lake temperatures in the Dead Sea for the period 1996–2010 (see discussion for details; from Gertman & Hecht, 2002; Gertman et al., 2010). The uncertainties are reported as both, standard error of the mean (SE; error bars), and 95% confidence intervals (black broken lines). CO layers highlighted by vertical bands. (C) Modern monthly monitored deep lake temperatures between 2004 and 2010 (blue squares; from Gertman et al., 2010). The vertical bands illustrate the approximate period during which the precipitation of CO halite crystals takes place on the deep lake floor

## 5 | DISCUSSION

The studied section of cumulate-coarse alternations provides insights into a short depositional period (*ca* 3 years) during which Lake Samra was most probably holomictic with a seasonal precipitation mechanism (Kiro et al., 2016). Another type (white, brown and black laminae with fine detritus and/or gypsum) of the layered ‘lh’ facies in core 5017-1-A has already been related to annual deposition cycles with periodicities of *ca* 11, 7–8, and 4–5 years (Palchan et al., 2017). However, the sampled section in this study lacks clear detrital layers and only consists of cumulate-coarse alternations. The fact that alternating detrital layers are missing indicates rather dry depositional conditions without flood events or increased runoff into Lake Samra during cumulate-coarse halite deposition (Ben Dor et al., 2019). However, the ‘lh’ facies type described by Palchan et al. (2017) is observed below and above the studied section in core 5017-1-A-122-2 (Figure 2B), indicating a full annually deposited sequence with changing hydrological parameters that drove halite precipitation and clastic deposition. Furthermore, the studied section can be considered a seasonal record of winter (cumulate halite) and summer (coarse halite) as previously observed in the modern Dead Sea (Sirota et al., 2016).

Only a few climate archives in the Levantine region (or in Europe) have revealed annual to seasonal temperature variability during MIS5e. The  $\delta^{18}\text{O}$  values and Sr/Ca ratios in corals from the Red Sea reported sea surface temperatures (SSTs) with a seasonal amplitude of 8.4°C at 122 ka (Felis et al., 2004), whereas pollen records enabled the reconstruction of seasonal temperature and moisture changes for the last 150 kyr (Chen & Litt, 2018). Based on their definition of pollen assemblage zones (PAZs) for core 5017-1-A, the sampled section at 315.15 m blf falls into the end of PAZ IV2 (340.6–313.7 m blf). This period marks the start of a transition from humid to dry conditions in the Levantine region by a progressive aridification, which is in line with the onset of the first halite deposition at the beginning of MIS5e (Chen & Litt, 2018). Furthermore, the authors report an initial warming starting in PAZ IV1 (313.7–290.2 m blf) judging by the significant pistachio

pollen increase at this time. Since the sampled section is slightly older, it is suggested that the obtained lake water temperatures of cumulate/coarse halite layers might still reflect relatively colder conditions under an increasing drying trend in the region.

Sedimentary records in Europe covering the MIS5e interval are more abundant. For instance, reconstructed mean temperatures of the coldest and warmest months in South-West Europe (Alboran Sea) allowed definition of the SST seasonality to 6–7.5°C on millennial timescales during the MIS5e, coevally with an increase in precipitation and highly evaporative summer conditions (Martrat et al., 2004). In southern Italy, a carbonate varved section of Lago Grande di Monticchio (127.20 ka; associated with the onset of MIS5e) exhibits a rapid increase in *Quercus* pollen (128.85 ka) and abundant pollen of Mediterranean woody taxa (Brauer et al., 2007). This has been interpreted as intervals of hot summers, seasonal moisture deficiency and high fire frequency, associated with peak summer insolation (Brauer et al., 2007). Alternatively, speleothems from the Soreq Cave reported an increase in annual rainfall on centennial scales at the onset of the MIS5e, associated with frost-free winters and drought-free summers in the Levantine region (Bar-Matthews et al., 2000). Most of these records, however, are missing a precise quantification of the interpreted palaeoseasonality.

Annually grown halite layers in the Dead Sea can be used to overcome such limitations by considering modern halite deposits as an analogue for the abundant halite layers in DSDDP core 5017-1-A (Figure 2A). The onset of modern CO halite growth coincides with a seasonal transition, when lake bottom temperatures are comparatively colder during winter (Sirota et al., 2017). A subsequent hypolimnetic warming during the summer has been shown in recent works, with maximum values attained each year during late summer and a seasonal difference of around 1°C between early and late summer lake bottom temperatures (Arnon et al., 2016; Gertman et al., 2010; Sirota et al., 2016). The results of this study follow this pattern with increasing hypolimnetic temperatures from the base to the top of CO halite layers in DSDDP core 5017-1-A-122-2 (with an increase of 3.0, 4.6 and 1.5°C for



**TABLE 1** Measured entrapment temperatures in halite fluid inclusions. Columns provide the sediment core depth in metres below lake floor (m blf), the number of fluid inclusions per sample (N), the averaged entrapment temperature per sample (Mean  $T_x$ ), the standard deviation of a sample population (SD), and the standard error of the mean (SE). Both lower and upper boundaries of 95% confidence intervals of each sample mean calculated with Student's *t*-test. Coarse sampled were corrected for hydrostatic pressure (Mean  $T_f$ ) (see Methods). Mean  $T_f$  values were not determined for cumulate halite samples (N.A.).

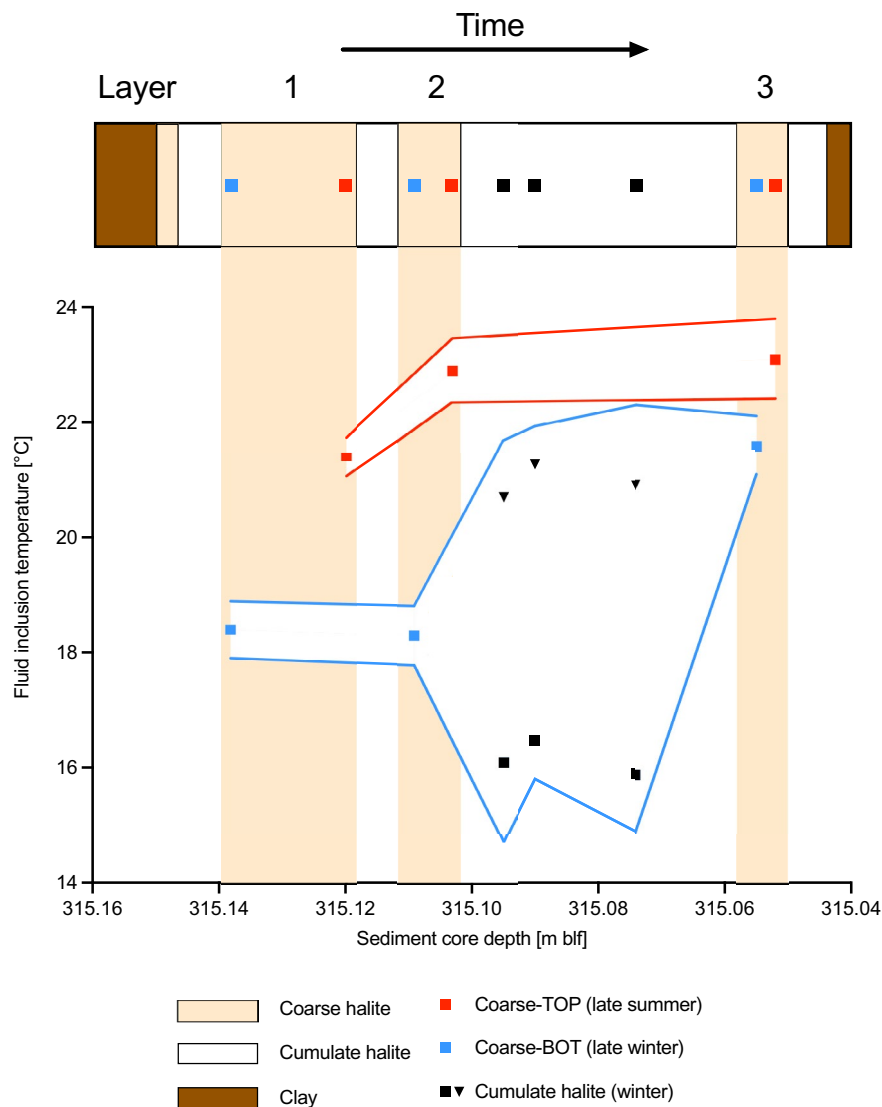
Sample name	Halite facies	Depth in core 5017-1 (m blf)	Section depth (cm)	N	Mean $T_x$ (°C)	SD (°C)	SE (°C)	Lower 95% CI (°C)	Upper 95% CI (°C)	Mean $T_f$ (°C)	Lower 95% CI (°C)	Upper 95% CI (°C)
CO3-TOP	Coarse	315.052	2.2	31	18.3	3.9	0.7	16.9	19.7	23.1	21.7	24.5
CO3-BOT	Coarse	315.055	2.5	17	16.8	2.1	0.5	15.7	17.9	21.6	20.5	22.7
CU4-C	Cumulate	315.074	4.4	15	15.9	3.9	1.0	13.7	18.1	N.A.	N.A.	N.A.
CU4-B	Cumulate	315.090	6.0	26	16.5	3.4	0.7	15.1	17.9	N.A.	N.A.	N.A.
CU4-A	Cumulate	315.095	6.5	14	16.1	5.2	1.4	13.0	19.1	N.A.	N.A.	N.A.
CO2-TOP	Coarse	315.103	7.3	21	18.1	2.6	0.6	16.9	19.3	22.9	21.7	24.1
CO2-MID	Coarse	315.105	7.5	35	15.1	2.4	0.4	14.3	15.9	19.9	19.1	20.7
CO2-BOT	Coarse	315.109	7.9	34	13.5	3.0	0.5	12.4	14.5	18.3	17.2	19.3
CO1-TOP	Coarse	315.120	9.0	37	16.6	2.1	0.4	16.0	17.4	21.4	20.8	22.2
CO1-MID	Coarse	315.124	9.4	40	16.9	2.6	0.4	16.0	17.7	21.7	20.8	22.5
CO1-BOT	Coarse	315.138	10.8	26	13.6	2.5	0.5	12.6	14.6	18.4	17.4	19.4

CO1, CO2 and CO3, respectively; Figure 3B). Hence, CO top samples can be interpreted as palaeo-summer halite precipitates. Accordingly, CO bottom samples (i.e. CO1-BOT, CO2-BOT, CO3-BOT) most probably recorded cold (late winter and early spring) hypolimnetic temperatures. The results thus highlight that holomictic periods in Lake Samra must have been associated with coarse halite precipitation in summer and seasonal temperature variations in the hypolimnion.

Further support for large seasonal water temperature differences can be found in cumulate halite samples and their modern analogues: the Dead Sea starts mixing in late November–early December today, with both a cooling of the brine and a (nearly coeval) increase in NaCl saturation which drives nucleation of cumulate halite in the homogeneous water column (Sirota et al., 2017). Thus, the lower  $T_x$  values obtained in cumulate halite FIs can be considered as seasonal winter records in this study (Figures 3B and 4). This is further in line with higher palaeotemperatures in both surrounding coarse halite samples CO2-TOP and CO3-BOT, which reflect the end and the onset of two successive summer seasons, respectively (Figures 3B and 4). However, it is important to note that the uncorrected cumulate  $T_x$  values do not picture the factual palaeoseasonal temperature variations with respect to the surrounding coarse layers. Since the initial (absolute) water depth of cumulate halite nucleation remains unknown, only the lower ( $=T_x$ ; *ca* 16°C) and upper boundary ( $=T_x + 4.8$ °C; *ca* 20.8°C) can be estimated for the studied cumulate layer. Hence, the palaeoseasonality would range between *ca* 2–7°C which prevents the absolute temperature differences from being assessed quantitatively, for example, between early spring/deep winter and late summer/deep winter. The focus, therefore, will be on entrapment temperatures obtained from coarse halite samples.

In accordance with this, the averaged  $T_f$  of coarse-bottom samples ( $19.4 \pm 1.1$ °C), which reflects late winter water/early spring lake bottom temperatures, is lower than the present-day lake bottom temperature in winter of *ca* 23°C. On the contrary, the averaged  $T_f$  of coarse-top samples ( $22.5 \pm 1.1$ °C) is close to present-day mean summer maxima (23.8°C for the period 1996–2010; Figure 3B). The offset between palaeo-late winter and present-day winter values of *ca* 4°C could be explained by an enhanced seasonality during MIS5e. A lower winter insolation (200 W/m<sup>2</sup> versus present day 220 W/m<sup>2</sup>) and enhanced summer insolation at both 30° and 35° North at that time may have driven the regional climate towards colder winters over the south and central Levant (Kiro et al., 2017; Torfstein et al., 2015). This is in line with climate simulations that showed a southward shift of winter storm track rains in the Mediterranean Basin and the Levant, linked with a strengthened Siberian anticyclone that pushed

**FIGURE 4** (Above) Sketch illustrating the annual depositional cycles in sediment core section 5017-1-A-122-2 with sub-sample locations. (Below) Temperature offset between grouped data in terms of the interpreted growth period: deep winter cumulate halite (uncorrected  $T_x$ , black squares; corrected  $T_f$ , triangles), late winter/early spring coarse halite (blue squares), and late summer coarse halite (red squares). Note that the corrected cumulate data reflect maximal potential palaeo lake temperatures, and thus should be considered with caution (see text for more details). Coloured (red and blue) envelopes are presented as the standard error of the mean. Vertical bands indicate growth season of coarse halite crystals on the deep lake floor



colder air farther south in Europe (Kutzbach et al., 2020). Furthermore, the climate model indicated slightly wetter winters and no change or even drier conditions at times of precession-caused high seasonality (*ca* 125 ka) in summertime (Kutzbach et al., 2020). Interestingly, a stronger palaeoseasonality was also reported in Red Sea corals during the peak of MIS5e based on increased sea surface temperatures (with seasonal cycles of 8.4°C at 122 ka), compared to a modern seasonal amplitude ranging between 4.5 and 5.6°C (Felis et al., 2004). The weaker modern seasonality in the Levant and eastern Mediterranean Sea region has been associated with enhanced winter insolation and lower summer insolation in the Northern Hemisphere during the Holocene (Kiro et al., 2017).

The modern amplitude of seasonality, measured as the difference between winter and summer lake bottom water temperatures, exhibits a nearly constant value of 1.5°C for the period 1996–2010 (Figure 3C). This modern seasonal thermal amplitude is thus at least half lower than the reconstructed seasonal amplitude from coarse halite data

for the MIS5e (Figures 3 and 4). The results therefore suggest a stronger palaeoseasonality during MIS5e, with distinct differences in entrapment temperatures between the bottom and the top of each coarse halite layer (Figure 4).

## 6 | CONCLUSIONS

Using the speed of sound in halite fluid inclusions from the DSB, this study reconstructs lake bottom temperatures of Lake Samra during marine isotope stage (MIS) 5e. As demonstrated by three successive coarse halite layers, palaeotemperatures increased between the bottom (late winter/spring) and the uppermost (late summer) sampling interval of each coarse layer. Conversely, three sub-samples of a fine cumulate halite layer yield stable and lower (deep winter) temperature values, highlighting that the alternation of coarse and cumulate halite layers in core 5017-1 reflect seasonal contrasts of lake bottom waters under holomictic conditions during MIS5e. These

data further imply that the reconstructed seasonal amplitude of lake bottom water temperatures at the onset of MIS 5e in Lake Samra was at least twice as high as the modern amplitude of seasonality.

Hence, this study clearly highlights the potential of using BS to investigate primary FIs in annual salt layers and reconstruct palaeotemperature variations in lacustrine sediment cores, at a seasonal resolution. Moreover, using BS on base-top halite crystals from multiple halite layers does not require any preparation of thin sections, is easily applied on small FIs, and can provide a reasonable quantity of  $T_x$  measurements. Thus, future studies dealing with (palaeo) Dead Sea-like hydroclimates should focus on coarse salt layers to reconstruct the seasonal variability of lake temperatures on decadal to millennial scales.

### ACKNOWLEDGEMENTS

We thank M. Schwab and A. Brauer from GFZ Potsdam (Germany) and the Dead Sea Deep Drilling Project members for providing core material of sediment core DSDDP-5017-1-A. We appreciate the constructive feedbacks of two anonymous reviewers who largely improved the manuscript. This study is part of the PhD thesis of NB and was funded by Campus France during the national research program MOPGA.

### CONFLICT OF INTEREST

The authors declare no competing interests.

### AUTHOR CONTRIBUTIONS

NSB, EG, VG and FC developed the concept of the study. EG sampled the bulk core material. NSB sampled the core section and prepared the samples. NSB conducted the measurements and produced the entrapment temperature data. FC, EG and NSB analysed the data. NSB created the figures. All authors contributed to the main text, interpretations of data and finalised the manuscript.

### DATA AVAILABILITY STATEMENT

The data that support the findings of this study are available on request from the corresponding author. The data are not publicly available due to privacy or ethical restrictions.


### ORCID

Niels S. Brall  <https://orcid.org/0000-0001-8345-4793>

Véronique Gardien  <https://orcid.org/0000-0001-9707-2980>

Daniel Ariztegui  <https://orcid.org/0000-0001-7775-5127>

Philippe Sorrel  <https://orcid.org/0000-0003-0074-5961>

Emmanuel Guillermin  <https://orcid.org/0000-0002-2725-9229>

Frédéric Caupin  <https://orcid.org/0000-0002-8892-2514>

### REFERENCES

- Anati, D.A. & Stiller, M. (1991) The post-1979 thermohaline structure of the Dead Sea and the role of double-diffusive mixing. *Limnology and Oceanography*, *36*, 342–353.
- Anati, D.A., Stiller, M., Shasha, S. & Gat, J.R. (1987) Changes in the thermo-haline structure of the Dead Sea: 1979–1984. *Earth and Planetary Science Letters*, *84*, 109–121.
- Ariztegui, D., Anselmetti, F.S., Robbiani, J.-M., Bernasconi, S.M., Brati, E., Gilli, A. & Lehmann, M.F. (2010) Natural and human-induced environmental change in southern Albania for the last 300 years – Constraints from the Lake Butrint sedimentary record. *Global and Planetary Change*, *71*, 183–192.
- Arnon, A., Selker, J.S. & Lensky, N.G. (2016) Thermohaline stratification and double diffusion diapycnal fluxes in the hypersaline Dead Sea. *Limnology and Oceanography*, *61*, 1214–1231.
- Baldini, J.U.L., Lechleitner, F.A., Breitenbach, S.F.M., van Hunen, J., Baldini, L.M., Wynn, P.M., Jamieson, R.A., Ridley, H.E., Baker, A.J., Walczak, I.W. & Fohlmeister, J. (2021) Detecting and quantifying palaeoseasonality in stalagmites using geochemical and modelling approaches. *Quaternary Science Reviews*, *254*, 106784.
- Bar-Matthews, M., Ayalon, A., Gilmour, M., Matthews, A. & Hawkesworth, C.J. (2003) Sea-land oxygen isotopic relationships from planktonic foraminifera and speleothems in the Eastern Mediterranean region and their implication for paleorainfall during interglacial intervals. *Geochimica et Cosmochimica Acta*, *67*, 3181–3199.
- Bar-Matthews, M., Ayalon, A. & Kaufman, A. (2000) Timing and hydrological conditions of Sapropel events in the Eastern Mediterranean, as evident from speleothems, Soreq cave, Israel. *Chemical Geology*, *169*, 145–156.
- Ben Dor, Y., Neugebauer, I., Enzel, Y., Schwab, M.J., Tjallingii, R., Erel, Y. & Brauer, A. (2019) Varves of the Dead Sea sedimentary record. *Quaternary Science Reviews*, *215*, 173–184.
- Brauer, A., Allen, J.R.M., Mingram, J., Dulski, P., Wulf, S. & Huntley, B. (2007) Evidence for last interglacial chronology and environmental change from Southern Europe. *Proceedings of the National Academy of Sciences*, *104*, 450–455.
- Brauer, A., Dulski, P., Mangili, C., Mingram, J. & Liu, J. (2009) The potential of varves in high-resolution paleolimnological studies. *PAGES News*, *17*, 96–98.
- Brocas, W.M., Felis, T., Gierz, P., Lohmann, G., Werner, M., Obert, J.C., Scholz, D., Kölling, M. & Scheffers, S.R. (2018) Last interglacial hydroclimate seasonality reconstructed from tropical Atlantic corals. *Paleoceanography and Paleoclimatology*, *33*, 198–213.
- Chen, C. & Litt, T. (2018) Dead Sea pollen provides new insights into the paleoenvironment of the southern Levant during MIS 6–5. *Quaternary Science Reviews*, *188*, 15–27.
- Chu, G., Liu, J., Schettler, G., Li, J., Sun, Q., Gu, Z., Lu, H., Liu, Q. & Liu, T. (2005) Sediment fluxes and varve formation in Sihailongwan, a maar lake from northeastern China. *Journal of Paleolimnology*, *34*, 311–324.
- Clemens, S.C. & Prell, W.L. (2003) A 350,000 year summer-monsoon multi-proxy stack from the Owen Ridge, Northern Arabian Sea. *Marine Geology*, *201*, 35–51.

- Denton, G.H., Alley, R.B., Comer, G.C. & Broecker, W.S. (2005) The role of seasonality in abrupt climate change. *Quaternary Science Reviews*, 24, 1159–1182.
- Felis, T., Lohmann, G., Kuhnert, H., Lorenz, S.J., Scholz, D., Pätzold, J., Al-Rousan, S.A. & Al-Moghrabi, S.M. (2004) Increased seasonality in Middle East temperatures during the last interglacial period. *Nature*, 429, 164–168.
- Francus, P., von Suchodoletz, H., Dietze, M., Donner, R.V., Bouchard, F., Roy, A.-J., Fagot, M., Verschuren, D. & Kröpelin, S. (2013) Varved sediments of Lake Yoa (Ounianga Kebir, Chad) reveal progressive drying of the Sahara during the last 6100 years. *Sedimentology*, 60, 911–934.
- Gertman, I. & Hecht, A. (2002) The Dead Sea hydrography from 1992 to 2000. *Journal of Marine Systems*, 35, 169–181.
- Gertman, I., Kress, N., Katsenelson, B. & Zavialov, P. (2010) Equations of state for the Dead Sea and Aral Sea: Searching for common approaches. Israel Oceanographic and Limnological Research (IOLR) Report IOLR/12. Accessed December 2021.
- Goldstein, S.L., Kiro, Y., Torfstein, A., Kitagawa, H., Tierney, J. & Stein, M. (2020) Revised chronology of the ICDP Dead Sea deep drill core relates drier-wetter-drier climate cycles to insolation over the past 220 kyr. *Quaternary Science Reviews*, 244, 106460.
- Guillerm, E. (2019) Turning halite fluid inclusions into accurate paleothermometers with Brillouin spectroscopy: development of a new method and application to the Last Interglacial in the Dead Sea. (These de doctorat). Lyon
- Guillerm, E., Gardien, V., Ariztegui, D. & Caupin, F. (2020) Restoring halite fluid inclusions as an accurate palaeothermometer: Brillouin thermometry versus microthermometry. *Geostandards and Geoanalytical Research*, 44, 243–264.
- Huguet, C., Kim, J.H., Sinninghe Damste, J.S. & Schouten, S. (2006) Reconstruction of sea surface temperature variations in the Arabian Sea over the last 23 kyr using organic proxies (TEX86 and U37K'). *Paleoceanography*, 21, PA3003.
- Kiro, Y., Goldstein, S.L., Garcia-Veigas, J., Levy, E., Kushnir, Y., Stein, M. & Lazar, B. (2017) Relationships between lake-level changes and water and salt budgets in the Dead Sea during extreme aridities in the Eastern Mediterranean. *Earth and Planetary Science Letters*, 464, 211–226.
- Kiro, Y., Goldstein, S.L., Lazar, B. & Stein, M. (2016) Environmental implications of salt facies in the Dead Sea. *Bulletin of the Geological Society of America*, 128(5–6), 824–841.
- Kutzbach, J.E., Guan, J., He, F., Cohen, A.S., Orland, I.J. & Chen, G. (2020) African climate response to orbital and glacial forcing in 140,000-y simulation with implications for early modern human environments. *Proceedings of the National Academy of Sciences*, 117, 2255–2264.
- Labuhn, I., Tell, F., von Grafenstein, U., Hammarlund, D., Kuhnert, H. & Minster, B. (2021) A modern snapshot of the isotopic composition of lacustrine biogenic carbonates: Records of seasonal water temperature variability. EGU General Assembly Conference Abstracts, EGU21-13178.
- Liu, J. & An, Z. (2020) Leaf wax *n*-alkane carbon isotope values vary among major terrestrial plant groups: Different responses to precipitation amount and temperature, and implications for paleoenvironmental reconstruction. *Earth-Science Reviews*, 202, 103081.
- Martrat, B., Grimalt, J.O., Lopez-Martinez, C., Cacho, I., Sierro, F.J., Flores, J.A., Zahn, R., Canals, M., Curtis, J.H. & Hodell, D. (2004) Abrupt temperature changes in the Western Mediterranean over the past 250,000 years. *Science*, 306, 1762–1765.
- Mekki-Azouzi, M.E., Tripathi, C.S.P., Pallares, G., Gardien, V. & Caupin, F. (2015) Brillouin spectroscopy of fluid inclusions proposed as a paleothermometer for subsurface rocks. *Scientific Reports*, 5, 1–9.
- Milner, A.M., Collier, R.E., Roucoux, K.H., Müller, U.C., Pross, J., Kalaitzidis, S., Christanis, K. & Tzedakis, P.C. (2012) Enhanced seasonality of precipitation in the Mediterranean during the early part of the Last Interglacial. *Geology*, 40, 919–922.
- Neev, D. & Emery, K.O. (1967) *The Dead Sea: depositional processes and environments of evaporites*. Jerusalem: Geological Survey Israel Bulletin, 41, 147 pp.
- Neugebauer, I., Brauer, A., Schwab, M.J., Waldmann, N.D., Enzel, Y., Kitagawa, H., Torfstein, A., Frank, U., Dulski, P., Agnon, A., Ariztegui, D., Ben-Avraham, Z., Goldstein, S.L., Stein, M. & Scientific Party, D.S.D.D.P. (2014) Lithology of the long sediment record recovered by the ICDP Dead Sea Deep Drilling Project (DSDDP). *Quaternary Science Reviews*, 102, 149–165.
- Ojala, A.E.K., Kosonen, E., Weckström, J., Korkkonen, S. & Korhola, A. (2013) Seasonal formation of clastic-biogenic varves: the potential for palaeoenvironmental interpretations. *GFF – Special Issue: Varve Genesis, Chronology and Paleoclimate*, 135, 237–247.
- Palchan, D., Neugebauer, I., Amitai, Y., Waldmann, N.D., Schwab, M.J., Dulski, P., Brauer, A., Stein, M., Erel, Y. & Enzel, Y. (2017) North Atlantic controlled depositional cycles in MIS 5e layered sediments from the deep Dead Sea basin. *Quaternary Research*, 87, 168–179.
- Riechelmann, D.F., Riechelmann, S., Wassenburg, J.A., Fohlmeister, J., Schöne, B.R., Jochum, K.P., Richter, D.K. & Scholz, D. (2020) High-resolution proxy records from two simultaneously grown stalagmites from Zoolithencave (southeastern Germany) and their potential for palaeoclimate reconstruction. *Geochemistry, Geophysics, Geosystems*, 21, e2019GC008755.
- Shi, J., Cook, E.R., Lu, H., Li, J., Wright, W.E. & Li, S. (2010) Tree-ring based winter temperature reconstruction for the lower reaches of the Yangtze River in southeast China. *Climate Research*, 41, 169–175.
- Sirota, I., Arnon, A. & Lensky, N.G. (2016) Seasonal variations of halite saturation in the Dead Sea. *Water Resources Research*, 52, 7151–7162.
- Sirota, I., Enzel, Y. & Lensky, N.G. (2017) Temperature seasonality control on modern halite layers in the Dead Sea: In situ observations. *GSA Bulletin*, 129, 1181–1194.
- Sirota, I., Enzel, Y., Mor, Z., Ben Moshe, L., Eyal, H., Lowenstein, T.K. & Lensky, N.G. (2021) Sedimentology and stratigraphy of a modern halite sequence formed under Dead Sea level fall. *Sedimentology*, 68, 1069–1090.
- Smit, J., Brun, J.P., Fort, X., Cloething, S. & Ben-Avraham, Z. (2008) Salt tectonics in pull-apart basins with application on the Dead Sea. *Tectonophysics*, 449, 1–16.
- Stein, M. (2001) The sedimentary and geochemical record of Neogene-Quaternary water bodies in the Dead Sea Basin – inferences for the regional paleoclimatic history. *Journal of Paleolimnology*, 26, 271–282.
- Stein, M., Ben-Avraham, Z., Goldstein, S., Agnon, A., Ariztegui, D., Brauer, A., Haug, G., Ito, E. & Yasuda, Y. (2011) Deep drilling at the Dead Sea. *Scientific Drilling*, 11, 46–47.
- Steinhorn, I. (1983) In situ salt precipitation at the Dead Sea. *Limnology and Oceanography*, 28, 580–583.



- Steinhorn, I. (1985) The disappearance of the long term meromictic stratification of the Dead Sea. *Limnology and Oceanography*, 30, 451–472.
- Torfstein, A., Goldstein, S.L., Kushnir, Y., Enzel, Y., Haug, G. & Stein, M. (2015) Dead Sea drawdown and monsoonal impacts in the Levant during the last interglacial. *Earth and Planetary Science Letters*, 412, 235–244.
- Torfstein, A., Goldstein, S., Stein, M. & Enzel, Y. (2013) Impacts of abrupt climate changes in the Levant from Last Glacial Dead Sea levels. *Quaternary Science Reviews*, 69, 1–7.
- Trachsel, M., Kamenik, C., Grosjean, M., McCarroll, D., Moberg, A., Brázdil, R., Büntgen, U., Dobrovolný, P., Esper, J., Frank, D.C., Friedrich, M., Glaser, R., Larocque-Tobler, I., Nicolussi, K. & Riemann, D. (2012) Multi-archive summer temperature reconstruction for the European Alps, AD 1053–1996. *Quaternary Science Reviews*, 46, 66–79.
- Waldmann, N., Stein, M., Ariztegui, D. & Starinsky, A. (2009) Stratigraphy, depositional environments and level reconstruction of the last interglacial Lake Samra in the Dead Sea basin. *Quaternary Research*, 72, 1–15.
- Wang, M., Zong, Y., Zheng, Z., Man, M., Hu, J. & Tian, L. (2018) Utility of brGDGTs as temperature and precipitation proxies in subtropical China. *Scientific Reports*, 8, 194.
- Werner, M., Mikolajewicz, U., Heimann, M. & Hoffmann, G. (2000) Borehole versus isotope temperatures on Greenland: seasonality does matter. *Geophysical Research Letters*, 27, 723–726.
- Wirth, S.B., Gilli, A., Simonneau, A., Ariztegui, D., Vannière, B., Glur, L., Chapron, E., Magny, M. & Anselmetti, F.S. (2013) A 2000 year long seasonal record of floods in the southern European Alps. *Geophysical Research Letters*, 40, 4025–4029.

## SUPPORTING INFORMATION

Additional supporting information may be found in the online version of the article at the publisher's website.

**How to cite this article:** Brall, N.S., Gardien, V., Ariztegui, D., Sorrel, P., Guillerm, E. & Caupin, F. (2022) Reconstructing lake bottom water temperatures and their seasonal variability in the Dead Sea Basin during MIS5e. *The Depositional Record*, 00, 1–12. Available from: <https://doi.org/10.1002/dep2.185>